Cardiovascular Engineering and Technology, Vol. 6, No. 1, March 2015 *(© 2014)* pp. 80–91
DOI: 10.1007/s13239-014-0195-5

Hemodynamics in Normal and Diseased Livers: Application of Image-Based Computational Models

STEPHANIE M. GEORGE,[1] LISA M. ECKERT,[1] DIEGO R. MARTIN,[2] and DON P. GIDDENS[3]

[1]Department of Engineering, East Carolina University, 225 Slay Building, Mail Stop 117, Greenville, NC 27858-4353, USA; [2]Department of Radiology, University Medical Center, University of Arizona, 1501 North Campbell Ave., P.O. Box 245067, Tucson, AZ 85724, USA; and [3]Wallace H. Coulter Department of Biomedical Engineering, Georgia Institute of Technology and Emory University, 313 Ferst Drive, Room 3112, Atlanta, GA 30332-0535, USA

(Received 7 April 2014; accepted 10 September 2014; published online 23 December 2014)

Associate Editor Steven C. George oversaw the review of this article.

Abstract—This investigation demonstrates the utility of image-based computational models in portal venous hemodynamics. The long-term objective is to develop methodologies based upon noninvasive imaging and hemodynamic computational models for blood flow in major vessels of the liver that will significantly augment and improve current practices in clinical care. Magnetic resonance imaging (MRI) and computational fluid dynamics (CFD) were used to investigate liver hemodynamics. MRI data were obtained in 7 healthy subjects and 4 patients diagnosed with cirrhosis, and computational models were developed and validated for two healthy subjects and two patients. Additional simulations of post-prandial hemodynamics and portal hypertension were completed. The MRI studies identified several new parameters (portal vein V_{avg}/total liver volume, V_{var}, splenic vein flow rate per total liver volume, and % splenic flow/portal vein flow) that offer statistical differentiation between healthy subjects and patients with liver disease. Computational models were used to calculate the contribution of blood supply to the right and left lobes of the liver derived from the superior mesenteric vein (greater in healthy subjects vs. patients); and simulate post-prandial conditions and progressive portal hypertension. CFD offers a tool to test hypotheses without the acquisition of additional data and elucidate hemodynamic effects as disease progresses. In addition, several new MRI derived parameters have been identified as having promise to distinguish between healthy and patient groups and, potentially, to monitor disease progression.

Keywords—Portal vein, Magnetic resonance imaging, Computational fluid dynamics, Cirrhosis.

INTRODUCTION

Diseases of the liver, including hepatitis C, non-alcoholic fatty liver disease and liver cancer, present major health problems that affect over 30 million Americans of all ages and ethnicities[1] and cause over 30,000 deaths annually.[15] It is estimated that up to 25% of people in the U.S. may have non-alcoholic fatty liver disease, representing an additional looming threat to public health. Diseases such as primary biliary cirrhosis, primary sclerosing cholangitis, and autoimmune hepatitis affect fewer people but are concentrated in women and have devastating consequences. Liver disease diagnosis is accomplished through liver function tests; and, once detected, life style changes and medications that slow disease progression are treatment modalities. However, chronic disease that leads to irreversible scarring, or cirrhosis, requires liver transplantation; and since the need for donated livers far exceeds the supply, early diagnosis and treatment are critical.

While liver diseases arise from various causes including viruses, toxins, and genetics, one common manifestation is altered hemodynamics. The liver is an organ with a complex, dual blood supply as illustrated in Fig. 1.[13] The portal vein (PV) provides the majority of blood to the liver (~80%) while the hepatic artery (HA) supplies the remainder. The PV forms from a confluence of the splenic vein (SV), which drains the spleen, and the superior mesenteric vein (SMV), which drains the digestive tract. Before entering the liver, the PV splits into the right and left branches. The liver is drained by the hepatic vein. Chronic liver disease results from changes in tissue architecture that cause an increase in resistance to blood flow in the lobes of

Address correspondence to Stephanie M. George, Department of Engineering, East Carolina University, 225 Slay Building, Mail Stop 117, Greenville, NC 27858-4353, USA. Electronic mail: georges@ecu.edu

the liver, leading to an elevated pressure in the PV and resulting in portal hypertension (PH). The PV is unique in that it is situated between two capillary beds, the digestive tract and the liver, and thus it is not possible to measure pressure in the PV directly. Clinically, a hepatic venous pressure gradient based on the invasively measured wedge pressure in the hepatic vein (difference between wedge hepatic venous pressure and free hepatic venous pressure) is used to determine PH.[2] Additional hemodynamic consequences of liver disease include dilation of the PV, decreased PV velocity, enlarged spleen with increased splanchnic circulation, varices and ascites.[12] In addition to hemodynamic changes, a notable anatomic change is enlargement of the left lobe of the liver, which grows to compensate for the asymmetric nature of liver disease that characteristically is more advanced in the right lobe. One hypothesis for this asymmetry is that disease initiation and progression in the right lobe are due to the composition of the blood that supplies that lobe. Since blood in the SMV comes from the digestive tract, it carries substances absorbed during digestion, including toxins, such as alcohol, known to damage the liver. After eating, blood flow in the SMV and hence to the liver increases, carrying both nutrients and toxins arising from digestion. If the right portal vein (RPV) contains a disproportionate blood flow originating from the SMV, this could support the hypothesis.

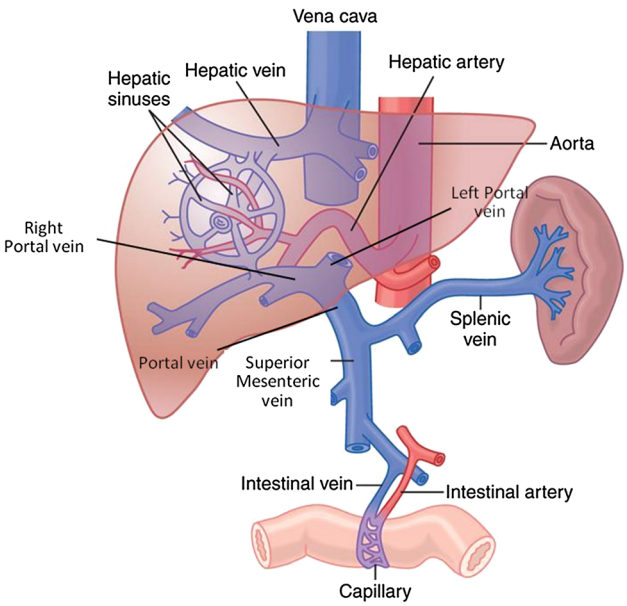

FIGURE 1. Liver circulation.[13] The splenic and superior mesenteric veins join to form the portal vein which splits into the right and left portal vein branches. The liver is also supplied by the hepatic artery which joins the venous flow at the capillary level before being collected into the hepatic vein which drains into the inferior vena cava.

Flow in the major vessels supplying blood to the liver has not been studied as thoroughly as in other vessels such as the carotid and coronary arteries, and there is a great need for better characterization of both physiologic and pathologic flows. Noninvasive hemodynamic investigations of the liver employing magnetic resonance imaging (MRI) are used increasingly and offer the ability to acquire high resolution anatomic and velocity data. Previous studies have quantified PV hemodynamics utilizing phase contrast MR (PC-MR) in healthy subjects and patients with various forms of liver disease,[11,16,21,25,30] and 4D-MR has been employed to elucidate time varying flow patterns.[7,20,22–24] While these investigations have demonstrated the potential for non-invasive hemodynamic assessment, definitive parameters that can be used as measures of disease state and progression have not been established; and large variability in PV flow has been reported for both healthy subjects and patients, with somewhat conflicting results. For example, PV flow in patients with liver cirrhosis showed no significant difference from healthy subjects in one study,[11] while in another investigation, significant differences between healthy subjects and patients were demonstrated under normal respiration and when subjects were breath-holding after expiration.[25] The feasibility of employing time-resolved 4D-MR to measure blood flow in the PV and its tributaries has been explored,[22,24] and these studies suggest excellent potential for noninvasive interrogation of flow. However, investigations in 24 patients with cirrhosis showed no correlation between flow in the vessels of the PV circulation and MELD score[7]; and studies in 17 patients and 7 normal subjects showed large variability in flow rates, making it difficult to define parameters that differentiate between patients and healthy subjects.[20] Further, contributions of extrahepatic vessels to the PV flow, such as the SV/PV ratio, have not been discussed. Differences between hepatic blood flows under fasting and post-prandial conditions have been investigated using MR and Doppler ultrasound with increases in PV flow being documented following food intake, as expected.[14,21,26,27] Taourel *et al.*[26] found that the postprandial response was significantly decreased in patients with cirrhosis, suggesting that pre- and post-prandial studies may allow for stress testing of portal hemodynamics as a benchmark for monitoring disease progression.

Only limited computational modeling of PV hemodynamics has been reported in the literature. Previous investigations have modeled the hepatic circulation using electrical analogues to optimize device settings for hypothermic perfusion systems.[6,28] Additional studies have investigated the microcirculatory blood flow in the lobule, the functional unit of the liver.[5,19] There has been some development of computational

fluid dynamics (CFD) models in the PV; however, these are limited to idealized models,[18] a single healthy subject,[3,9] and uncertainty analyses.[17] In the last few years there have been a small number of clinical CFD models generated including a single subject before and after the transjugular intrahepatic portosystemic shunt (TIPS) procedure[10] and a single subject hepatectomy case.[8] Thus, there is a need for developing computational approaches that enable more thorough investigations of liver hemodynamics in healthy and disease states.

The goals of the present study are (i) to compare several MR-derived variables in healthy subjects and patients with liver cirrhosis in a search for candidate parameters that might prove useful in describing disease progression and (ii) to employ MR image-based CFD as a companion technology for augmenting MR in the management of patients. Although 4D-MR can produce geometry and fluid velocity maps, MR alone is not capable of exploring variations in hemodynamic parameters unless measurements are repeated, nor can it simulate different hypothetical scenarios as a predictive tool. In this investigation we employ CFD to aid in interpretation of MR data, to determine the sources of blood flowing to each lobe of the liver, and to simulate parametrically the effects of eating and portal hypertension (increased right lobe pressure) upon PV hemodynamics.

METHODS

Subject Selection

This study includes data from seven healthy volunteers (1 male, 6 females) ages 24–28 (25.9 ± 1.3) with no previous or current diagnosis of liver disease and four patients (2 males, 2 females) ages 50–63 (55 ± 5.7). The patients were selected from among those scheduled for an abdominal MRI with a diagnosis of cirrhosis, MELD scores ranging from 11 to 13, and no tumors present. All subjects were instructed to fast at least 2 h prior to the scan. The study was approved by the Emory University Institutional Review Board.

Imaging

Magnetic resonance imaging of all subjects was performed on either a Philips 1.5T Intera system (Philips Healthcare, Andover, MA) or a Siemens Avanto 1.5T system (Siemens AG, Erlangen, Germany), both equipped with a body phased array coil. Scans were completed with the subjects in a supine position and began with short reconnaissance scans using balanced fast field echo (BFFE) to locate the PV. The vessel geometry including the SMV, SV, complete PV, and the right and left PV branches (RPV and LPV) was scanned using either the BFFE or the steady-state free precession technique (SSFP). The scans were breath-held (~20 s) contiguous slices of 3 mm thickness with a resolution of 1.37 × 1.37 mm, which permitted adequate accuracy for vessel geometry reconstruction for CFD models. A series of coronal images was acquired to allow for segmentation of the liver lobes.

PC-MR scans were taken to acquire time-resolved velocity distributions that provided flow boundary conditions for CFD calculations. These scans were performed during the same session using ECG leads or a peripheral pulse unit for cardiac vector cardiogram gating, and velocity data were gathered using a segmented gradient echo sequence obtained from the mid-PV with the imaging plane placed 90° to the long axis. PC-MR scans were also acquired for the SMV and SV before their confluence to the PV and for the RPV or LPV just after the PV bifurcation. Only the axial velocity component was measured due to time constraints, but this allowed the velocity information to be employed to calculate flow rates. Scan parameters were as follows: slice thickness 6–8 mm, resolution of 1.17 × 1.17 mm, TR 24.2, TE 8, number of phases 16–20, and Venc 30–60 cm/s. An example geometry showing the sites of PC-MR acquisition is presented in Fig. 2.

For subjects whose geometry was acquired over several breath-holds, image registration was necessary, and segmentation techniques were applied to the geometry data sets to identify the lumen boundary as described in.[29] Briefly, the segmentation process created serial contours in space within the vessel geometry, allowing for the reconstruction of a smooth surface. The vessel lumens were also segmented for the PC-MR scans using the magnitude portions of the images and threshold criteria in the region of interest. Next, the segmented magnitude images were employed as a mask to multiply the phase images, leaving only the velocity information of interest. The velocity intensities were then converted to actual velocity values employing a MATLAB program developed for this application, resulting in axial velocity values (over a cross-section as well as the cardiac cycle), flow rates, and luminal areas. Liver volume was calculated by manually segmenting the liver and summing volumes of the voxels.

CFD Models

CFD models were developed for two healthy subjects and two patients with best data quality. The geometry obtained from MR data was used to create a

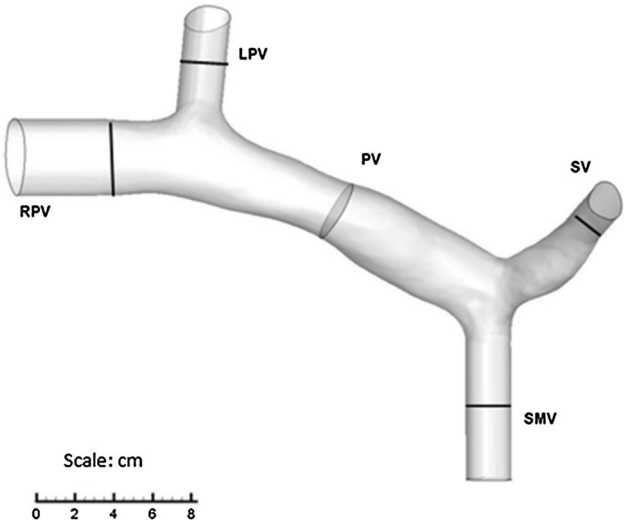

FIGURE 2. Image reconstruction of the PV geometry in a healthy subject, with the lines indicating sites of PC-MR velocity acquisition. The PC-MR data from the RPV, SMV, and SV were used as boundary conditions for the CFD models, while the PV data were used for validation of the computed velocity results.

non-uniform rational B-spline surface employing Geomagic (Geomagic USA, Morrisville, NC, USA). The geometry was additionally cropped and smoothed, and this surface was then imported into Gambit (ANSYS, Inc., Canonsburg, PA, USA) where the outlets and inlets were extended and a tetrahedral mesh was created with a mesh size of 0.1 mm. A grid sensitivity analysis was performed by decreasing the mesh size to ensure appropriate resolution for the grid. The velocity at the center of the PV was used as a marker to determine grid sensitivity.

The governing equations for the CFD model were the incompressible continuity and Navier–Stokes equations which were solved numerically using a commercial software package, FLUENT (ANSYS, Inc., Canonsburg, PA, USA). The assumed fluid properties were representative of blood (density, $\rho = 1060$ kg/m^3, viscosity coefficient, $\mu = 0.035$ Poise). Ho *et al.*[9] found that defining blood as a Newtonian fluid is a good assumption in the PV. The boundary conditions necessary for the model include vessel geometry (Fig. 2), inlet (SMV and SV) velocities, and outflow flow splits (RPV and LPV). The inlet vessels were extended by at least 1 diameter with a mean extension of 2.3 diameters to reduce artificial inlet effects. The inlet velocities were assumed to be blunt and were calculated from PC-MR derived flow rates and geometric area. Flow was measured in the RPV, and flow in the LPV was assumed to be equal to the flow in the PV minus flow in the RPV. If the subject had a trifurcation, the remaining flow was divided between the two remaining outlets based on area. Two outlet boundary conditions were run and compared: (i) measured outflow and (ii) outlet pressures using targeted mass flow rate. The outlets were extended to reduce artificial end effects. The CFD results were displayed in Tecplot (Tecplot, Inc., Bellevue, WA), allowing for visualization of velocity profiles and streamtraces. Validation of the CFD models was obtained by comparison of average velocity with PC-MR data at the mid-PV.

Flow in these liver vessels was expected to be only marginally pulsatile, with little variation over the cardiac cycle.[20,25] Our own PC-MR findings confirmed this, as shown for a healthy subject (N9) in Panel (a) of Fig. 3.To examine the effects of unsteadiness on computed flow field parameters we used PC-MR unsteady flow measurements as boundary conditions for subject N9 and computed the velocity field. The unsteady solver was pressure based with first order implicit formulation using the Green-Gauss node based gradient option. Pressure–velocity coupling was defined by SIMPLE, and the discretization methods for pressure and momentum were standard and first order upwind, respectively. Two cardiac cycles were computed with only data from the second cycle used for comparisons. Panel (b) of Fig. 3 presents calculated velocity profiles at a cross section in the center of the PV at three different times (average flow, maximum flow and minimum flow) obtained from the unsteady computations and compares these with the steady state calculations using the average velocity at these times. Although there are small differences in velocity profiles, the steady velocity magnitudes are within 0.1–1.2% of the unsteady values. This similarity is reflected in panel (c) of Fig. 3 where we compare the cross-sectional averaged velocities obtained from the fully unsteady and the quasi-steady assumptions. Based on these findings, we used steady flow CFD results in our

subsequent comparisons with time averaged MR-derived parameters.

One concept explored by CFD was motivated by the question of whether contributions of SMV and SV blood to the right and left lobes may be different between normal subjects and those with PH. Thus, the fraction of flow from the SMV that fed the RPV (or LPV) branch was calculated using a method described by Dasi *et al.*[4] Utilizing TECPLOT to analyze the CFD results, streamtraces were initiated in a grid-like pattern over a cross-sectional slice of the SMV. The flow rate contribution for each streamtrace was calculated by multiplying the velocity at the streamtrace origin by the individual grid area. The outlet (RPV or LPV) for each streamtrace was determined using a C program written for this purpose, and the SMV blood that contributed flow to each outlet was determined by summing the flow from each streamtrace.

As discussed previously, CFD may prove useful in modeling changes in liver hemodynamics in specific individuals, both as related to normal hemodynamic variations and also to departures from physiologic flows as liver disease progresses. For postprandial simulations we parametrically increased the flow in the SMV, noting that Sadek, *et al.*, found that PV flow rate increased between 24 and 74% after eating.[21] To model this response in our subjects, increases of 25, 50, and 75% of the baseline PV flow were added to the SMV flow rate measured by PC-MR. Since these studies are hypothetical and no PC-MR flow split data were available for the outlets, the SV inlet flow was kept constant at its PC-MR measured value, and the outlet pressure boundary condition was applied using the pressure from the baseline case. For simulating PH we increased the RPV pressures in the healthy subjects systematically in equal increments while keeping the inlet pressures and LPV outlet pressure constant at levels corresponding to the baseline calculation.

Data Analysis

MR image data were employed to compute anatomical parameters, including vessel cross-sectional area and liver lobe volume. To compute an overall average velocity, V_{avg}, at a slice, velocity voxels were averaged over the cross-section at each time interval

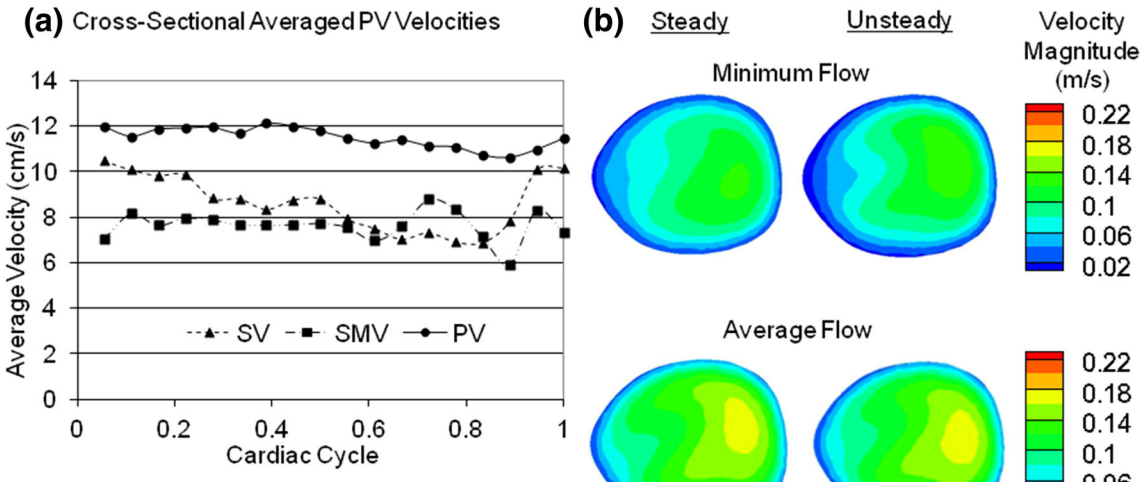

(c) N9 Cross-Sectional Averaged PV Velocity

Case	Steady Velocity (cm/s)	Unsteady Velocity (cm/s)
Min. Flow	7.62	7.68
Average Flow	10.9	10.77
Max. Flow	13.83	13.82

FIGURE 3. Quasi-Steady Analysis Results. (a) There was little variation in PC-MR measured cross-sectional average velocity with time in the PV, SMV and SV. (b) Computed velocity profiles in the PV were very similar when comparing fully unsteady computations with a quasi-steady assumption. (c) Time-varying PV velocities averaged over the cross section closely correlated well with steady velocities.

and then averaged over the entire cardiac cycle. For computation of flow rate, Q_{avg}, the flow through each voxel was calculated and all voxels were summed and averaged over the cardiac cycle. We computed a velocity variance (V_{var}) by averaging the velocities over the cross section at each time interval and then taking the difference between the maximum and minimum of these values. Because of time and technical limitations during the MRI procedures, not all parameters were able to be measured in all subjects, and specific group numbers are referenced in the results section. An Exact Wilcoxian test was performed to determine statistically significant differences in parameters between the healthy and patient groups. This test was chosen because the assumption of normal distributions is not made.

RESULTS

Our studies involved three components: (i) MR investigations of seven healthy subjects and four patients with liver cirrhosis; (ii) CFD modeling for two healthy subjects and two patients; and (iii) CFD simulations of post-prandial hemodynamics (two healthy subjects and two patients) and portal hypertension (two healthy subjects).

MR Results

Locations of MR and PC-MR measurement slices are shown in Fig. 2, and measured flows in the major vessels were found to be quasi-steady, as presented in Fig. 3. We used the period of one cardiac cycle as a reference over which to compute time averaged PC-MR results, as summarized in Table 1. The area of the PV was significantly larger in patients than in healthy subjects (patients, 1.75 ± 0.49 cm^2; healthy subjects, 0.97 ± 0.08 cm^2, $p = 0.006$). The PV velocity averaged over the cross section was 12.74 ± 3.17 cm/s and 8.74 ± 3.09 cm/s for the healthy subjects and patients, respectively. Although this difference did not reach statistical significance, it did show a trend for decreased PV velocity in patients. There was no significant difference in PV flow rate in patients vs. normal subjects (1032 ± 586 mL/min vs. 783 ± 241 mL/min). There were little velocity and flow rate changes over the cardiac cycle, but this lack of variability was more notable in the patients, i.e., the velocity variance, V_{var}, was significantly different between patients and healthy subjects (1.93 ± 1.0 cm/s vs. 4.4 ± 1.7 cm/s, $p = 0.024$). To examine variations in the amount of blood required by the tissue, the velocity and flow rate were each divided by the total liver volume. Interestingly, the PV flow/liver volume was similar in both groups (patients, 0.641 ± 0.187 mL/min/cm^3; healthy subjects, 0.583 ± 0.175 mL/min/cm^3), but the ratio of PV velocity/liver volume was significantly lower in patients (0.0058 ± 0.0017 cm/s/cm^3 vs. 0.01 ± 0.0025 cm/s/cm^3, $p < 0.05$).

The splenic vein (SV) drains blood from the spleen, which can become enlarged with cirrhosis. This was seen in our study where the SV area was larger in patients, ($1.18 + 0.37$ cm^2 vs. $0.578 + 0.1$ cm^2, $p = 0.024$). There was no difference in SV average velocity between groups (patients, 8.88 ± 1.65 cm/s; healthy subjects, 7.93 ± 1.53 cm/s), but the average flow rate was greater in patients (666 ± 311 mL/min vs. 300 ± 102 mL/min, $p = 0.024$). When expressed as SV flow/liver volume, the patients again had significantly greater values (0.46 ± 0.163 mL/min/cm^3 vs. 0.202 ± 0.033 mL/min/cm^3, $p = 0.019$). The ratio of SV flow to PV flow was also calculated, and results show that patients had a significantly increased ratio (0.74 ± 0.32 vs. 0.36 ± 0.069, $p = 0.0095$). There were no significant differences between healthy subjects and patients in any of the SMV variables examined.

CFD Results: Healthy Subjects and Patients

Computational models were developed for two healthy subjects and two patients. The CFD velocity results at a center section in the PV were compared to PC-MR data for these four subjects and the computed values were within 0.5–27% of the PC-MR values, with subject N3 having the greatest difference (Table 2). Differences in assumptions on boundary conditions, e.g., outflow split vs. outlet pressure, did not affect the computed PV average velocity (differences ~0.02–0.17 cm/s).

Because of interest in how SMV and SV flows contribute to the right and left lobes of the liver, the CFD models were also used to calculate the percentages of SMV blood that flowed to the RPV and LPV, and the results are presented in Table 3. For the healthy subjects the majority of the SMV flow went to the RPV, while for patients the SMV flow was more evenly divided between RPV and LPV.

The computational analyses revealed complicated flow patterns in the PV with secondary or swirling flow in both healthy subjects and patients, and there was substantially more mixing of blood from the SV and SMV sources in the patients, as demonstrated by the computed streamtraces seen in Fig. 4 where examples from a healthy subject (N9) and a patient (D6) are presented in the left panel for baseline conditions.

CFD Simulations: Post-prandial Flow and Portal Hypertension

We simulated postprandial hemodynamics by increasing the SMV flow by 25, 50 and 75%, while

TABLE 1. Results for MR-derived parameters in the portal venous system.

	Healthy subjects	Patients	*p* value
Portal vein (PV)	$n = 7$	$n = 4$	
Average area (cm^2)*	0.97 ± 0.08	1.75 ± 0.49	0.0061
Average velocity (V_{avg}) (cm/s)	12.74 ± 3.17	8.74 ± 3.09	0.1636
V_{avg}/total liver volume ($cm/s/cm^3$)*	0.01 ± 0.0025	0.0058 ± 0.0017	0.0416
Velocity variance (V_{var})* (cm/s)	4.4 ± 1.7	1.93 ± 1	0.0242
Average flow rate (Q_{avg}) (mL/min)	783 ± 241	1032 ± 586	0.6485
Q_{avg}/total liver volume ($mL/min/cm^3$)	0.583 ± 0.175	0.641 ± 0.187	0.7619
Splenic vein (SV)	$n = 7$	$n = 4$	
SV area (cm^2)*	0.578 ± 0.1	1.18 ± 0.37	0.0061
SV V_{avg} (cm/s)	7.93 ± 1.53	8.88 ± 1.65	0.4121
SV Q_{avg} (mL/min)*	300 ± 102	666 ± 311	0.0242
SV Q_{avg}/total liver volume* ($mL/min/cm^3$)	0.202 ± 0.033	0.46 ± 0.163	0.019
	$n = 6$	$n = 4$	
PV blood composition (SV/PV)*	0.36 ± 0.069	0.74 ± 0.32	0.0095

* Indicates a statistically significant difference $p < 0.05$.

TABLE 2. Comparison of the CFD model with MR results.

Subject	CFD—outflow BC PV average velocity (cm/s)	CFD—pressure BC PV average velocity (cm/s)	MR PV average velocity (cm/s)
N3	7.01	6.98	9.55
N9	10.62	10.6	11.5
D4	8.89	9.06	8.97
D6	8.41	8.41	8.45

TABLE 3. Partition of SMV blood into the RPV and LPV as determined from CFD results.

Subject	% SMV flow to RPV	% SMV flow to LPV
N3	94.3	8.5
N9	66.4	33.3
D4	48	54.2
D6	49.4	47

holding SV flow constant. The right panel of Fig. 4 illustrates changes in streamtraces for a normal subject (N9) and a patient (D6) when PV flow is increased by 75% to simulate a postprandial state. There is considerably more secondary flow in both subjects by comparison with the baseline state, with the patient exhibiting extremely strong swirling patterns.

The percentage of SMV blood that ultimately goes to the RPV with increases in SMV flow was determined from computed streamtraces for each of the four subjects as shown in Fig. 5, with variable results. Subject N3, who had a high percentage of SMV flow feeding the RPV at baseline, showed a linear decrease in this parameter as SMV flow increased, while patient D4 showed an opposite trend. On the other hand, there was no apparent trend in N9 and D6, and the small number of subjects prevents a statistical comparison.

In the PH simulation the RPV pressure was increased in the two healthy subjects, N3 and N9, while holding SMV and SV inflow pressures as well as the LPV outflow pressure constant at their baseline values. The LPV flow percentage increased, the RPV flow percentage decreased, and the PV flow decreased with an increase in RPV pressure. The relationship between the percentage decrease in pressure drop (caused by the increased RPV pressure assumption) and the percentage increase in LPV flow in each subject was found to be linear.

Figure 6 displays the computed velocity profiles at the mid-PV section for the two healthy subjects. For subject N3 the RPV outlet pressure is increased until flow reversal was seen in the RPV. There are shifts in the velocity profile patterns in these examples, but most noteworthy are the effects of increased RPV pressures on flow patterns in the outlet branches. Flow into the RPV is clearly impeded, and as shown by the streamtraces for N9, there is little flow going to the right lobe of the liver for this simulation.

DISCUSSION

This investigation demonstrates the feasibility of employing MRI derived geometry and flow velocity information from the PV blood vessel system in individual subjects to develop computational models that can be used to explore PV hemodynamics in normal and diseased states. We also compare differences in several MRI derived parameters of the PV system between healthy and patient groups. The potential utility of CFD to explore relevant hypothetical states is

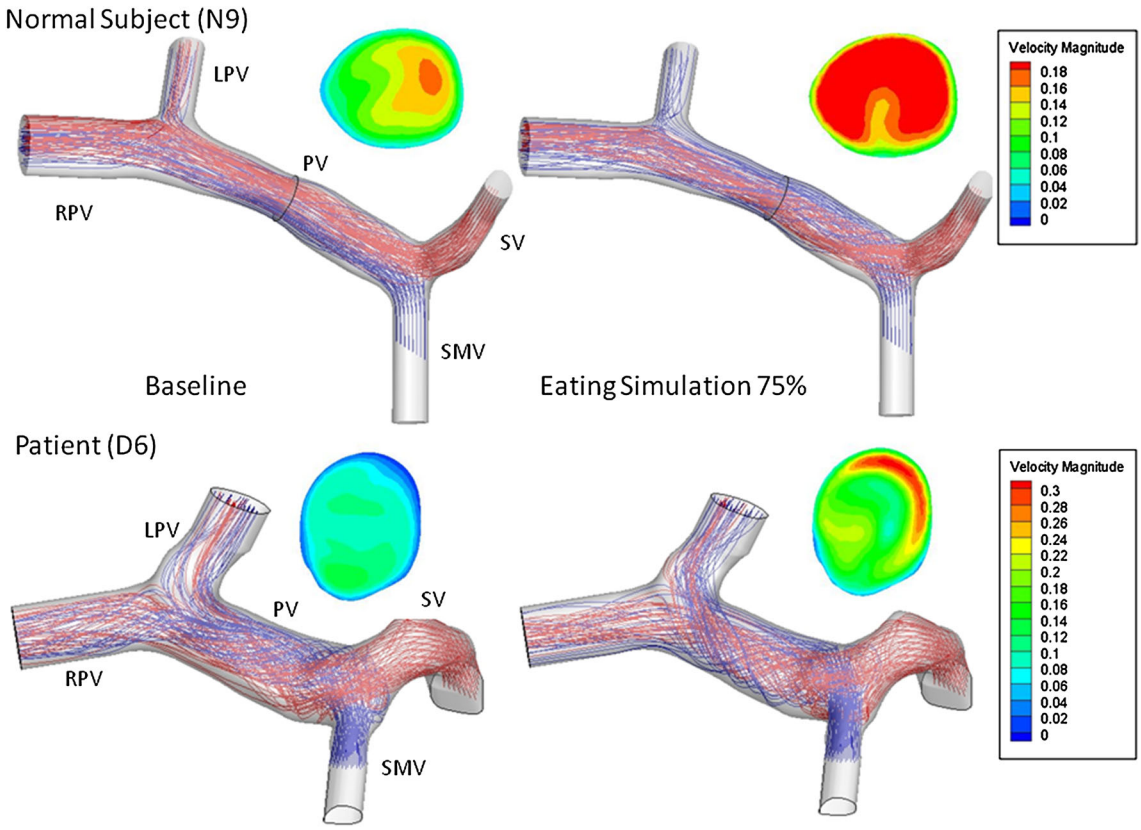

FIGURE 4. Streamtraces from CFD results for one healthy subject (N9) and one patient (D6) under baseline and simulated post-prandial conditions. The stronger secondary flow patterns in the patient, as well as the larger vessel diameter, are readily seen under both flow conditions. Changes in velocity profiles can also be seen.

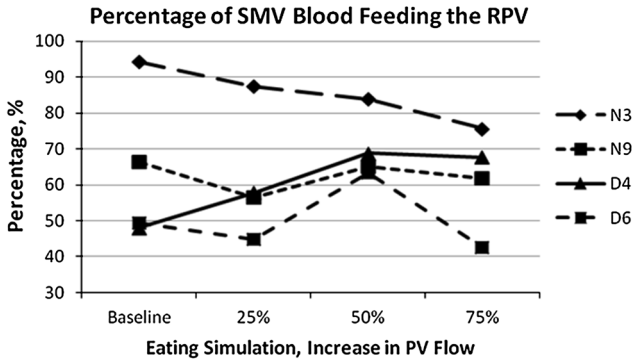

FIGURE 5. Percentage of SMV blood feeding the RPV at various increases in SMV flow. The increases in PV flow simulate a range of post-prandial states provided in the literature.[11,27]

demonstrated by simulating postprandial hemodynamics and portal hypertension without the need for additional imaging acquisition.

Our study population includes patients aged 50–63 and healthy subjects aged 24–28, which raises a question of possible age-related hemodynamic differences when comparing normal young subjects with older patients. Using 4D-MR, Stankovic, *et al.*,[22] demonstrated no significant difference in mean velocity, maximum velocity, flow volume, and vessel area of the SMV, SV, splenic-mesenteric confluence, RPV branch and LPV branch between healthy older subjects (mean age, 58.6 years ± 5.9; range, 50–69 years) and healthy young volunteers (mean age, 27.5 years ± 3.3; range, 22–37 years). The only exception was a significant decrease (0.05 m/s vs. 0.06 m/s) in the LPV mean velocity in healthy young volunteers when compared to healthy older subjects. Therefore, preliminary conclusions should not be affected by the age differences in our two study groups.

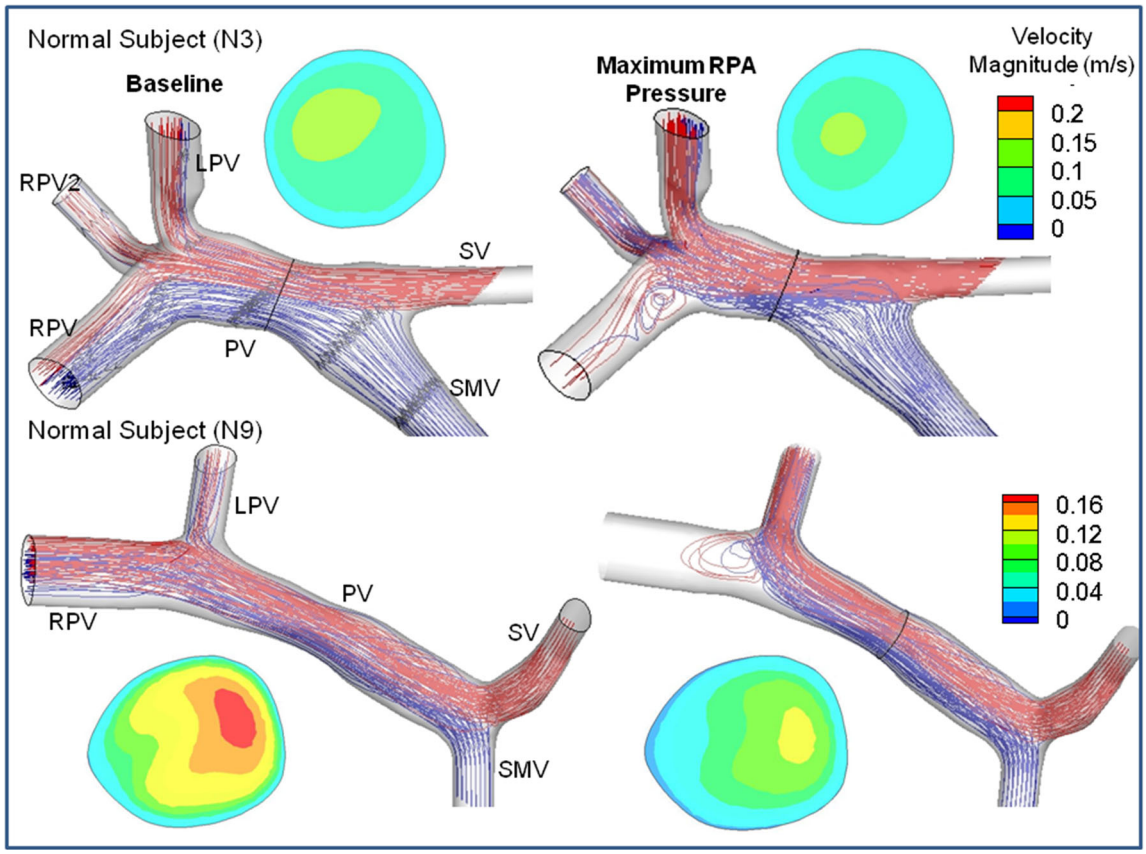

FIGURE 6. Streamtraces from CFD results for both healthy subjects (N3 and N9) under baseline and simulated RPV pressure increases. The reversed flow and secondary flow can be seen in both subjects, and velocity profile changes can also be seen.

Large variations in PV geometry have been reported in the literature, and both anatomy and flow were highly variable in our patients, as well as in the healthy subjects. Such geometric variability is expected to contribute to variability in velocity profiles in the PV, and profile skewing was commonly seen in the PC-MR velocity profiles, as well as in the four cases examined through CFD. From the computational viewpoint, both SMV and SV inflows as well as LPV and RPV outflows contribute to velocity profile skewing, since both upstream and downstream flow boundary conditions affect details in the region of interest. The computed velocities demonstrate that simple assumptions for velocity profiles in the PV, such as Poiseuille flow, can be inaccurate, and the strong secondary patterns suggest caution when interpreting flow data from Doppler ultrasound measurements.

As expected, a significant difference was found in PV cross sectional area between healthy subjects and patients, with the patients having larger lumens. Interestingly, the variability in PV area among healthy subjects was relatively small, while that of the patients was quite large—presumably reflecting patient variability in increased levels of PH arising from being in different stages of disease. The PV MR velocity measurements for healthy subjects in this study (12.74 ± 3.17 cm/s) are within the range reported in the literature.[14,16,24,25,30] Our PV flow rate (783 ± 241) is also within the range reported in literature.[14,22,23,25,30] When healthy subjects and patients in our study are considered, the V_{avg} per liver volume in the PV was significantly lower in patients which is a new finding not previously reported. Although there were no differences in flow per liver volume between healthy subjects and patients, the combination of increased liver volume and increased PV cross-sectional area in patients appears to have led to the observed significantly lower value of V_{avg} per liver volume in the patients.

While there was little pulsatility in PV flows by comparison to arterial flows, there were modest variations in velocity over a cardiac cycle, and we computed velocity variance, V_{var}, as previously described. One striking feature seen in this parameter was a significant difference between the healthy and patient groups (Table 1), with V_{var} being much greater in the healthy subjects ($p < 0.024$). This is possibly due to effects of PH in the patients, and this parameter may

offer information related to disease progression in an individual patient, although a larger sample size is required to establish any measure of utility.

Referring to Table 1, the area, flow rate, and flow rate per unit liver volume of the SV were significantly increased in patients. Cirrhosis can cause an increase in blood flow to the spleen and thus an increase in blood flow in the SV, so these parameters may prove useful in disease diagnosis and monitoring progression.

The contributions to PV blood flow arising from the SMV and SV tributaries were calculated and were consistent across all normal subjects in that the majority of the PV blood is from the SMV (Table 1). However, in patients the percentage of SV blood in the PV increased, which is again consistent with the increased spleen size and SV flow. By defining the ratio of SV flow to PV flow (SV/PV), the difference between healthy subjects and patients was statistically significant, and the variation among patients was much larger, likely reflecting different stages of disease.

The flow split between the RPV and LPV branches tended to shift to increase the proportion of blood flow into the LPV for the patients. Without the presence of disease one would expect a greater proportion of blood is required to supply the right lobe than the smaller left lobe. Liver disease primarily starts in the right lobe of the liver, increasing resistance on the right side and perhaps diverting some of the supply to the lower resistance left side, as seen in the CFD simulations. In addition, the left lobe of the liver may hypertrophy, increasing the demand for blood. This flow split parameter may be an important indicator that could be investigated more closely in future patient studies.

The use of CFD enables the creation of subject specific models from MRI data. The data set presented here, comprising only four subjects, is extremely limited, and general conclusions should not be drawn. In the present study four complete CFD models were created, two healthy subjects and two patients, and computed velocities compared well with PC-MR data acquired from the mid-point of the PV. These models were used to investigate blood flow patterns in the PV that resulted from the confluence of flows entering from the SMV and SV. Under the assumption of steady laminar flow, streamlines also represent particle path lines, so tracing streamlines (e.g., streamtraces) gives an indication of secondary flows as well as blood element trajectories. As seen in Fig. 4, the CFD calculations showed weak secondary or swirling flow in the PV of the healthy subjects and stronger secondary flow for the patients, likely due to the increase in resistance in the liver and to asymmetry in the inlets and outlets.

The CFD models were also used to determine the sources of blood to the right lobe of the liver where disease occurs preferentially. In the healthy subjects, the majority of the SMV blood fed the right side of the liver, while in patients the SMV blood fed both sides equally (Table 3). This finding from the CFD models is consistent with the hypothesis that "dirty" blood may contribute to liver disease in the right lobe at early stages. As disease progresses and RPV resistance increases, a shift of SMV blood contribution to the left lobe is consistent with bilateral disease progression. However, we emphasize that these results suggest the potential of computational modeling to elucidate factors in liver disease, but by no means provide conclusive proof of the "dirty blood" hypothesis. Additionally, as noted previously, SMV flow increases in the postprandial state, so that variations in flow contributions of the SMV and SV to the RPV and LPV are to be expected in both healthy subjects and patients.[6,19,28] When simulating disease by increasing RPV pressure in the two healthy subjects, the LPV flow percentage increased. Additionally, the PV flow decreased and the flow into the RPV became significantly impeded. While this result is intuitive, the potential to use computational modeling to assess redistribution of blood flow in the hepatic vessels with progressing disease is intriguing.

This investigation demonstrates a methodology that can be employed to explore subject specific MRI and CFD to investigate hemodynamic parameters in the liver in order to provide additional noninvasive information to assist in managing patients with chronic liver disease. Although the number of subjects is small, several MRI derived parameters have been identified as having promise to distinguish between healthy and patient groups and, potentially, to monitor disease progression as an adjunct to decision making on the urgency of organ transplantation. Those parameters that relate to the PV include PV cross-sectional area, PV velocity variance (V_{var}) during the cardiac cycle, and possibly V_{avg} and V_{avg}/liver volume. Parameters related to the SV that deserve further study are SV cross-sectional area, SV average flow rate, and SV average flow rate per unit liver volume. Further, patient specific CFD can be a powerful tool to investigate hemodynamic patterns in the PV complex, to test hypotheses related to the effects of distribution of SMV and SV blood to the separate lobes of the liver, and to elucidate hemodynamic effects as disease progresses.

ACKNOWLEDGMENTS

The authors would like to acknowledge the following for their support of this work; study volunteers, Puneet Sharma, PhD, Lakshmi Dasi, PhD, Jason

Brinkley, PhD, Megha Sinha and the Cardiovascular Fluid Mechanics Laboratory. Research was partially supported by the Georgia Research Alliance and the East Carolina University Division of Research and Graduate Studies.

STATEMENT OF HUMAN STUDIES

All procedures followed were in accordance with the ethical standards of the responsible committee on human experimentation (institutional and national) and with the Helsinki Declaration of 1975, as revised in 2000 (5). Informed consent was obtained from all patients for being included in the study. All procedures followed were in accordance with the ethical standards of the responsible committee on human experimentation (institutional and national).

STATEMENT OF ANIMAL STUDIES

No animal studies were carried out by the authors for this article.

CONFLICT OF INTEREST

Author Stephanie M. George, Author Lisa M. Eckert, Author Diego R. Martin, and Author Don. P. Giddens declare that they have no conflict of interest.

REFERENCES

[1]American Liver Foundation. Retrieved from http://www.liverfoundation.org/ on July 28, 2014.
[2]Annett, L., R. Materne, E. Danse, J. Jamart, Y. Horsmans, and B. E. Van Beers. Hepatic flow parameters measured with MR imaging and Doppler US: correlations with degree of cirrhosis and portal hypertension. *Radiology* 229(2):409–414, 2003.
[3]Botar, C. C., T. Vasile, S. Sfrangeu, S. Clichici, P. S. Agachi, R. Badea, P. Mircea, and M. V. Cristea. Validation of CFD simulation results in case of portal vein blood flow. *Comput. Aided Chem. Eng.* 28:205–210, 2010.
[4]Dasi, L. P., K. Whitehead, K. Pekkan, D. de Zelicourt, K. Sundareswaran, K. Kanter, M. Fogel, and A. P. Yoganathan. Pulmonary hepatic flow distribution in total cavopulmonary connections: extracardiac versus intracardiac. *J. Thorac. Cardiovasc. Surg.* 141(1):207–214, 2011.
[5]Debbaut, C., J. Vierendeels, C. Casteleyn, P. Cornillie, D. Van Loo, P. Simoens, L. Van Hoorebeke, D. Monbaliu, and P. Segers. Perfusion characteristics of the human hepatic microcirculation based on three-dimensional reconstructions and computational fluid dynamic analysis. *J. Biomech. Eng. Trans. ASME* 134(1), 2012.
[6]Debbaut, C., D. Monbaliu, C. Casteleyn, P. Cornillie, D. Van Loo, B. Masschaele, J. Pirenne, P. Simoens, L. Van Hoorebeke, and P. Segers. From vascular corrosion cast to electrical analog model for the study of human liver hemodynamics and perfusion. *IEEE Trans. Biomed. Eng.* 58(1):25–35, 2011.
[7]Frydrychowicz, A., B. R. Landgraf, E. Niespodzany, R. W. Verma, A. Roldán-Alzate, K. M. Johnson, O. Wieben, and S. B. Reeder. Four-dimensional velocity mapping of the hepatic and splanchnic vasculature with radial sampling at 3 tesla: a feasibility study in portal hypertension. *J. Magn. Reson. Imaging* 34(3):577–584, 2011.
[8]Ho, C., R. Lin, S. F. Tsai, R. H. Hu, P. C. Liang, T. W. H. Sheu, and P. Lee. Simulation of portal hemodynamic changes in a donor after right hepatectomy. *J. Biomech. Eng.* 132:041002-1-7, 2010.
[9]Ho, H., A. Bartlett, and P. Hunter. Non-Newtonian blood flow analysis for the portal vein based on a CT image. In: Abdominal Imaging. Computational and Clinical Applications. Berlin: Springer, 2012, pp. 283–291.
[10]Ho, H., K. Sorrell, L. Peng, Z. Yang, A. Holden, and P. Hunter. Hemodynamic analysis for transjugular intrahepatic portosystemic shunt (TIPS) in the liver based on a CT-image. *IEE Trans. Med. Imaging* 32(1):92–98, 2013.
[11]Kashitani, N., S. Kimoto, M. Tsunoda, T. Ito, T. Tsuji, A. Ono, and Y. Hiraki. Portal blood blow in the presence or absence of diffuse liver disease: measurement by phase contrast MR imaging. *Abdom. Imaging* 20(3):197–200, 1995.
[12]Kayacetin, E., D. Efe, and C. Dogan. Portal and splenic hemodynamics in cirrhotic patients: relationship between esophageal variceal bleeding and the severity of hepatic failure. *J. Gastroenterol.* 39(7):661–667, 2004.
[13]Liver Circulation. Retrieved from http://www.studyblue.com/notes/note/n/phys-gi-/deck/3159802 on July 23, 2014.
[14]Lycklama à Nijeholt, G. J., K. Burggraaf, M. N. Wasser, L. J. Schultze Kool, R. C. Schoemaker, A. F. Cohen, and A. de Roos. Variability of splanchnic blood flow measurements using MR velocity mapping under fasting and post-prandial conditions-comparison with echo-doppler. *J. Hepatol.* 26(2):298–304, 1997.
[15]Murphy, S., J. Xu, and K. Kochanek. Deaths: preliminary data for 2010. *Natl Vital Stat. Rep.* 60(4):1–52, 2012.
[16]Nanashima, A., S. Shibasaki, I. Sakamoto, E. Sueyoshi, Y. Sumida, T. Abo, T. Nagasaki, T. Sawai, T. Yasutake, and T. Nagayasu. Clinical evaluation of magnetic resonance imaging flowmetry of portal and hepatic veins in patients following hepatectomy. *Liver Int.* 26(5):587–594, 2006.
[17]Pereira, J. M. C., J. P. Serra e Moura, A. R. Ervilha, and J. C. F. Pereira. On the uncertainty quantification of blood flow viscosity models. *Chem. Eng. Sci.* 101:253–265, 2013.
[18]Petkova, S., A. Hossain, J. Naser, and E. Palombo. CFD modeling of blood flow in portal vein hypertension with and without thrombosis. In Third International Conference on CFD in the Minerals and Process Industries. 2003.
[19]Rani, H. P., T. W. Sheu, T. M. Chang, and P. C. Liang. Numerical investigation of non-newtonian microcirculatory blood flow in hepatic lobule. *J. Biomech.* 39(3):551–563, 2006.
[20]Roldán-Alzate, A., A. Frydrychowicz, E. Niespodzany, B. R. Landgraf, K. M. Johnson, O. Wieben, and S. B. Reeder. In vivo validation of 4D flow MRI for assessing the hemodynamics of portal hypertension. *J. Magn. Reson. Imaging* 37(5):1100–1108, 2012.
[21]Sadek, A. G., F. B. Mohamed, E. K. Outwater, S. S. El-Essawy, and D. G. Mitchell. Respiratory and post-prandial changes in portal flow rate: assessment by phase contrast MR imaging. *J. Magn. Reson. Imaging* 6(1):90–93, 2005.

[22]Stankovic, Z., Z. Csatari, P. Deibert, W. Euringer, P. Blanke, W. Kreisel, Z. Zadeh, F. Kallfass, M. Langer, and M. Markl. Normal and altered three-dimensional portal venous hemodynamics in patients with liver cirrhosis. *Radiology* 262(3):862–873, 2012.

[23]Stankovic, Z., Z. Csatari, P. Deibert, W. Euringer, B. Jung, W. Kreisel, J. Geiger, M. Russe, M. Langer, and M. Markl. A feasibility study to evaluate splanchnic arterial and venous hemodynamics by flow-sensitive 4D MRI compared with Doppler ultrasound in patients with cirrhosis and controls. *Eur. J. Gastroenterol. Hepatol.* 25(6):669–675, 2013.

[24]Stankovic, Z., A. Frydrychowicz, Z. Csatari, E. Panther, P. Deibert, W. Euringer, W. Kreisel, M. Russe, S. Bauer, M. Langer, and M. Markl. MR-based visualization and quantification of three-dimensional flow characteristics in the portal venous system. *J. Magn. Reson. Imaging* 32(2):466–475, 2010.

[25]Sugano, S., K. Yamamoto, K. I. Sasao, and M. Watanabe. Portal venous blood flow while breath-holding after inspiration or expiration and during normal respiration in controls and cirrhotics. *J. Gastroenterol.* 34(5):613–618, 1999.

[26]Taourel, P., P. Perney, M. Dauzat, B. Gallix, J. Pradel, F. Blanc, L. Pourcelot, and J. M. Bruel. Doppler study of fasting and postprandial resistance indices in the superior mesenteric artery in healthy subjects and patients with cirrhosis. *J. Clin. Ultrasound* 26(3):131–136, 1998.

[27]Tsukuda, T., K. Ito, S. Koike, K. Sasaki, A. Shimizu, T. Fujita, M. Miyazaki, H. Kanazawa, C. Jo, and N. Matsunaga. Pre-and postprandial alterations of portal venous flow: evaluation with single breath-hold three-dimensional half-fourier fast spin-echo MR imaging and a selective inversion recovery tagging pulse. *J. Magn. Reson. Imaging* 22(4):527–533, 2005.

[28]van der Plaats, A., N. A. 't Hart, G. J. Verkerke, H. G. D. Leuvenink, P. Verdonck, R. J. Ploeg, and G. Rakhorst. Numerical simulation of the hepatic circulation. *Int. J. Artif. Organs.* 27(3):222–230, 2004.

[29]Yang, Y., S. M. George, D. R. Martin, A. R. Tannenbaum, and D. P. Giddens. 3D modeling of patient-specific geometries of portal veins using MR images. In: Proceedings of IEEE EMBS Annual International Conference, 2006, pp. 5290–5293.

[30]Yzet, T., R. Bouzerar, J. D. Allart, F. Demuynck, C. Legallais, B. Robert, H. Deramond, M. E. Meyer, and O. Balédent. Hepatic vascular flow measurements by phase contrast MRI and Doppler echography: a comparative and reproducibility study. *J. Magn. Reson. Imaging* 31(3):579–588, 2010.